JOM, Vol. 71, No. 5, 2019
https://doi.org/10.1007/s11837-019-03428-5

Influence of Carbon Content on Aluminothermic Reduction of Ilmenite During Hot Pressing

SHENGMING LIU,[1,3] MIN CHEN,[2] and XUAN XIAO[2]

1.—College of Materials Science and Engineering, Xihua University, Chengdu 610039, China.
2.—College of Titanium and Vanadium, Panzhihua University, Panzhihua 617000, China.
3.—e-mail: lsmxmh@163.com

Al_2O_3-TiCN-Fe composites were successfully prepared by hot pressing using natural ilmenite, aluminum, and carbon. The process of aluminothermic reduction of ilmenite and the influence of carbon on the phase evolution, synthetic products, microstructure, and properties were investigated using x-ray diffraction (XRD) analysis, scanning electron microscopy (SEM), and mechanical analysis. The XRD results showed that the reduction process of the $FeTiO_3$-2Al system was a gradual deoxygenation process. In the $FeTiO_3$-2Al-xC systems, carbon participates in the reduction reaction to form TiN, which gradually transforms to TiCN. The carbon content had a great influence on the presence of titanium oxides during the reaction. In addition, the grain size of Al_2O_3, TiCN, and Fe phases became smaller as the carbon content was increased. When the carbon content was 0.88 mol, the synthesized products achieved comprehensive mechanical properties, i.e., bending strength and Vickers hardness of 375 MPa and 15.5 GPa, respectively.

INTRODUCTION

Ilmenite has attracted interest from many researchers worldwide because of its abundant reserves and richness in two important metal elements, i.e., Fe and Ti. Different types of composite materials can be obtained by chemical reactions between ilmenite and different reducing agents. Research studies have focused on carbon reduction,[1,2] metal reduction,[3,4] and combined reduction of metal and carbon.[5–7] Among these reductions, the chemical reaction between ilmenite, aluminum, and carbon has been investigated extensively to prepare Al_2O_3-TiC-Fe or Al_2O_3-TiCN-Fe composites in a nitrogen-containing atmosphere because Al_2O_3-TiC/TiCN-Fe ceramics have excellent mechanical properties, such as resistance to high temperature, wear, corrosion, and oxidation.[8,9]

Various techniques can be used to manufacture Al_2O_3-TiC/TiCN-Fe composites. Among these, in situ techniques have received extensive attention,[10–12] including mechanical alloying, reactive sintering, microwave heating, or self-propagating high-temperature synthesis. Reinforcement can be synthesized by the reaction in composites prepared by such in situ techniques, which then nucleate and grow spontaneously. Thus, the reinforcement surface is not polluted, the matrix and reinforcement show good compatibility, and the resulting material exhibits high interfacial bonding strength. In situ synthesis methods simultaneously eliminate the cumbersome pretreatment reinforcement process, simplifying the preparation process. These features lead to better mechanical properties compared with composites processed using traditional, ex situ approaches.[13–15]

Several studies have explored the $FeTiO_3$-Al-C system, mostly[10,16,17] focusing on preparation of Al_2O_3-TiC/TiCN-Fe composite powders, but the preparation, microstructure, and properties of such composites have not been investigated in depth. In some studies,[18–20] Al_2O_3-TiC/TiCN-Fe composites were synthesized through the $FeTiO_3$-Al-C system, but the phase evolution during the formation process has not yet been thoroughly investigated. In addition, many investigations[21–23] have focused on synthesis of Al_2O_3-TiC composite by TiO_2, mainly investigating the preparation of powders instead of materials. The reaction mechanism has not been further studied, and the reaction sequences, aluminum reduction processes, and effect of C on the reaction process, microstructure, and properties remain unclear.

(Published online March 12, 2019)

In the work presented herein, Al_2O_3-TiCN-Fe composites were synthesized by hot pressing using in situ reaction between natural ilmenite, aluminum, and carbon. The reaction process and mechanism of the $FeTiO_3$-2Al-xC systems during hot-pressing processes were explored using the carbon-free $FeTiO_3$-2Al system and carbon-containing $FeTiO_3$-2Al-0.5C and $FeTiO_3$-2Al-0.75C systems. The influence of carbon on the phase evolution, microstructure, and properties of the product was also studied.

EXPERIMENTAL PROCEDURES

Material Synthesis

Ilmenite (average particle size approximately 158.26 μm; Panzhihua Mineral, Panzhihua, China), aluminum (> 99% purity, < 80 μm), and graphite powder (> 99% purity, < 30 μm) were used as raw materials. Table I presents the chemical composition of ilmenite. Aluminum and graphite powder were used as the reducing agent. The mixtures were prepared in accordance with Eq. 1:

$$FeTiO_3 + 2Al + xC + \frac{1-x}{2}N_2 \rightarrow TiC_xN_{1-x} + Al_2O_3 + Fe \quad (1)$$

A vertical planetary ball mill (QM-3SP4; Nanjing T-Bota Scietech Instruments & Equipment Co., Ltd., Nanjing, China) was used to mill the mixture of ilmenite, aluminum, and graphite. Steel balls with different diameters (6 mm and 10 mm) were used in the milling operation. The ball-to-powder ratio was maintained at 12:1. Ball milling was performed at room temperature in air condition.

After milling, about 20 g of the mixture was placed into a graphite crucible in a hot-pressing sintering furnace, which was evacuated to vacuum then filled with flowing nitrogen. The atmosphere flow rate was 1 L/min. The samples were sintered at different temperatures (600–1400°C) for 30 min under pressure of 20 MPa to investigate the synthesis process.

Material Characterization

The as-milled powders and sintered samples were characterized by XRD analysis (D/MAX-1200; Rigaku Denki, Beijing, China) using Cu K_α radiation in the range 10°–90°. Peak positions were taken from the International Center for Diffraction Data database. Raw XRD data were refined and analyzed using the MDI Jade 6.0 program (Materials Data Incorporated, Livermore, CA, USA). Silicon powder (SRM640; National Institute of Standards and Technology, Gaithersburg, MD, USA) was used as external standard to correct for instrumental broadening. The experimental errors were reduced as much as possible by curve fitting. The sintered specimens were investigated by scanning electron microscopy (SEM, VEGA II LMU; Tescan, Brno, Czech Republic).

Table I. Chemical composition of ilmenite powder (wt.%)

Ti	Fe	Si	Mn	Al	Ca	Mg	O
31.18	22.47	1.57	1.81	0.56	0.049	0.072	Balance

Mechanical Performance Testing

The sintered specimens were cut into bars to measure the flexure strength. The final dimensions of these samples were 3 mm × 3 mm × 30 mm. The flexure strength of the samples was measured by a three-point bending method with a support roller span length of 20 mm and crosshead speed of 0.5 mm/min. The Vickers hardness (VH) was measured using Vickers indentation at load of 20 kg with dwell time of 15 s.

RESULTS AND DISCUSSION

Figure 1 shows the XRD patterns of ilmenite and as-milled $FeTiO_3$-2Al-xC (x = 0 mol, 0.25 mol, 0.5 mol, 0.75 mol, 0.88 mol, and 1 mol) powders. Figure 1a shows the XRD pattern of ilmenite powder. The only phases revealed in the XRD patterns were $FeTiO_3$, TiO_2, and $Fe_2Ti_3O_9$, suggesting that, in addition to $FeTiO_3$, TiO_2 and $Fe_2Ti_3O_9$ phases were present in this kind of ilmenite. Presence of $Fe_2Ti_3O_9$ also indicates a serious degree of weathering of ilmenite. In addition, the ilmenite powder contained element impurities such as Ca, Mg, Si, Mn, and Al. The specific chemical composition is presented in Table I. These impurity elements were not clearly shown by XRD due to their low concentrations. Figure 1b shows the XRD pattern of as-milled $FeTiO_3$-2Al powder. The XRD profiles

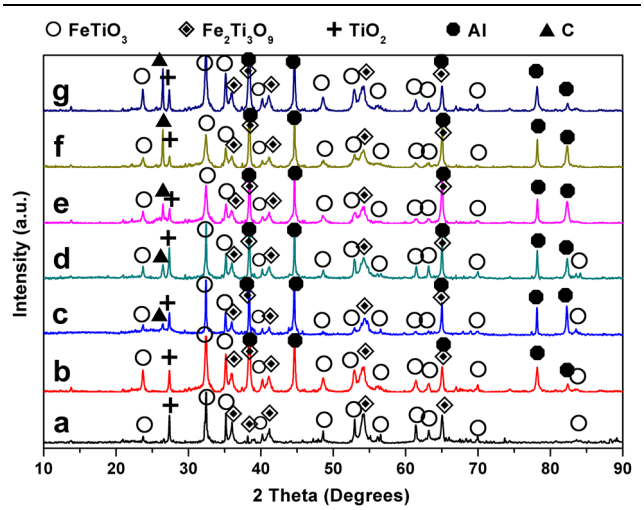

Fig. 1. XRD patterns of (a) ilmenite powders, and milled $FeTiO_3$-2Al-xC powders with x value of (b) 0 mol, (c) 0.25 mol, (d) 0.5 mol, (e) 0.75 mol, (f) 0.88 mol, and (g) 1 mol.

indicated that the milled powders contained $FeTiO_3$, TiO_2, $Fe_2Ti_3O_9$, and Al phases. No new peaks were present, suggesting that reactions between $FeTiO_3$, TiO_2, $Fe_2Ti_3O_9$, and Al did not occur on any significant scale during milling. The XRD patterns of the as-milled $FeTiO_3$-2Al-xC powders as a function of the carbon content are shown in Fig. 1c, d, e, f and g. The only phases shown by the XRD patterns were $FeTiO_3$, TiO_2, $Fe_2Ti_3O_9$, Al, and C. The intensity of the carbon peaks increased significantly with increase in the carbon content.

Influence of Carbon Content on the Reaction Process

To clarify the influence of the carbon content on the aluminothermic reduction process of ilmenite during the hot-pressing process, the carbon-free $FeTiO_3$-2Al and carbon-containing $FeTiO_3$-2Al-xC systems were investigated. The XRD results for each system after sintering at different temperatures are shown in Fig. 2, and all the phases present at each temperature from 600°C to 1400°C are listed in Table II.

Figure 2a shows the XRD patterns of as-milled $FeTiO_3$-2Al powder sintered at different temperatures for 0.5 h under pressure of 20 MPa and nitrogen atmosphere. No new phases appeared after heating the sample to 600°C, suggesting that no reaction occurred during heating to this temperature. The intensity of the TiO_2 peaks increased when the sample was heated to 700°C, suggesting that reaction of $Fe_2Ti_3O_9$, $FeTiO_3$, and Al forming TiO_2, Al_2O_3, and Fe occurred after melting of Al. The other product of the ilmenite reduction was iron. Unfortunately, the main peaks for iron were coangular with aluminum peaks and could not be deconvoluted, which is primarily due to the low intensity of the iron peaks that were expected to be present. In addition, two intermediate alloy phases appeared, i.e., Al_3Ti and $AlFe_3$. Many studies have reported an Al_3Ti phase, which was synthesized by the reaction of TiO_2 and Al.[21,22,24] Another intermediate alloy phase, $AlFe_3$, was formed by the reaction of residual aluminum with newly formed iron.

With a further temperature increase to 800°C, the amount of TiO_2 phase obviously increased, as shown by the corresponding increase of the relative peak intensities of the TiO_2, Al_2O_3, and Fe phases. Thus, the reaction between $Fe_2Ti_3O_9$, $FeTiO_3$, and Al continued from 700°C to 800°C. The ilmenite disappeared at this temperature, but the intermediate alloy phases, Al_3Ti and $AlFe_3$, were still present in the XRD patterns.

When the temperature was increased to 900°C, the intensity of the TiO_2 phase weakened, the intensity of the Al_2O_3 phase increased significantly, and the Ti_3O_5 phase appeared in the XRD patterns, suggesting that the reaction between TiO_2 and Al to form Ti_3O_5 and Al_2O_3 had already occurred. The peaks of the intermediate alloy phases, Al_3Ti and $AlFe_3$, became weak and then disappeared at 1000°C, which is due to the reaction between TiO_2 and these two intermediate alloy phases, as shown in Eqs. 2 and 3. The standard Gibbs free energy of formation for the reactions in Eqs. 2 and 3 is negative.

$$2Al_3Ti + 37TiO_2 = 13Ti_3O_5 + 3Al_2O_3 \quad \Delta G^\circ_{1000^\circ C} = -51\,kJ/TiO_2 \tag{2}$$

$$2AlFe_3 + 9TiO_2 = 3Ti_3O_5 + Al_2O_3 + 6Fe \quad \Delta G^\circ_{1000^\circ C} = -53\,kJ/TiO_2 \tag{3}$$

When the materials were heated to 1000°C, the intensity of the peaks corresponding to Ti_3O_5 and Al_2O_3 phases increased significantly while those for TiO_2 phase disappeared. When the temperature was increased from 1000°C to 1100°C, two significant changes in the XRD pattern were observed, i.e., the Ti_3O_5 and Fe phases disappeared, and the peaks of Ti_2O_3, TiO, Fe_2Ti, and Fe_3Ti_3O phases appeared. The appearance of Ti_2O_3, TiO, Fe_3Ti_3O, and Fe_2Ti can be assigned to the reaction between Ti_3O_5, Al, and Fe because of the disappearance of Ti_3O_5 and Fe, as shown in Eqs. 4–7. Thermodynamic data for Fe_3Ti_3O could not be found, thus the Gibbs free energy of the reaction generating Fe_3Ti_3O could not be obtained accurately. However, Fe_3Ti_3O can be approximately considered as $(Fe_2Ti)_{1.5}{\cdot}(Ti_{1.5}O)$. $Ti_{1.5}O$ lies between TiO and Ti in the order of valence, thus the Gibbs free energy of the reaction that generates Fe_3Ti_3O can be estimated as between − 310 kJ and − 412 kJ by Eqs. 5 and 7. As can be seen from Eqs. 4–7, the standard Gibbs free energy of these reactions is negative. In addition, Ti_2O_3 could also be obtained by the reaction between Ti_3O_5 and Al, as shown in Eq. 8. Although the energy of formation of Eq. 4 is more negative than that of Eq. 8, formation of Ti_2O_3 via Eq. 8 required 1/3 mol Ti_3O_5 compared with 4/3 mol Ti_3O_5 Al for Eq. 4. Khoshhal et al.[3] considered that the formation of Fe_2Ti in the $FeTiO_3$-2Al system is due to aluminothermic reduction of $FeTiO_3$ and TiO_2. However, in this work, the disappearance of Ti_3O_5 and Fe proves that the formation of Fe_2Ti was due to the reaction between Ti_3O_5, Al, and Fe.

$$3Ti_3O_5 + 4Al + 6Fe = 3Fe_2Ti + 3Ti_2O_3 + 2Al_2O_3 \quad \Delta G^\circ_{1000^\circ C} = -181\,kJ/Ti_3O_5 \tag{4}$$

$$6Ti_3O_5 + 14Al + 18Fe = 9Fe_2Ti + 9TiO + 7Al_2O_3 \quad \Delta G^\circ_{1000^\circ C} = -310\,kJ/Ti_3O_5 \tag{5}$$

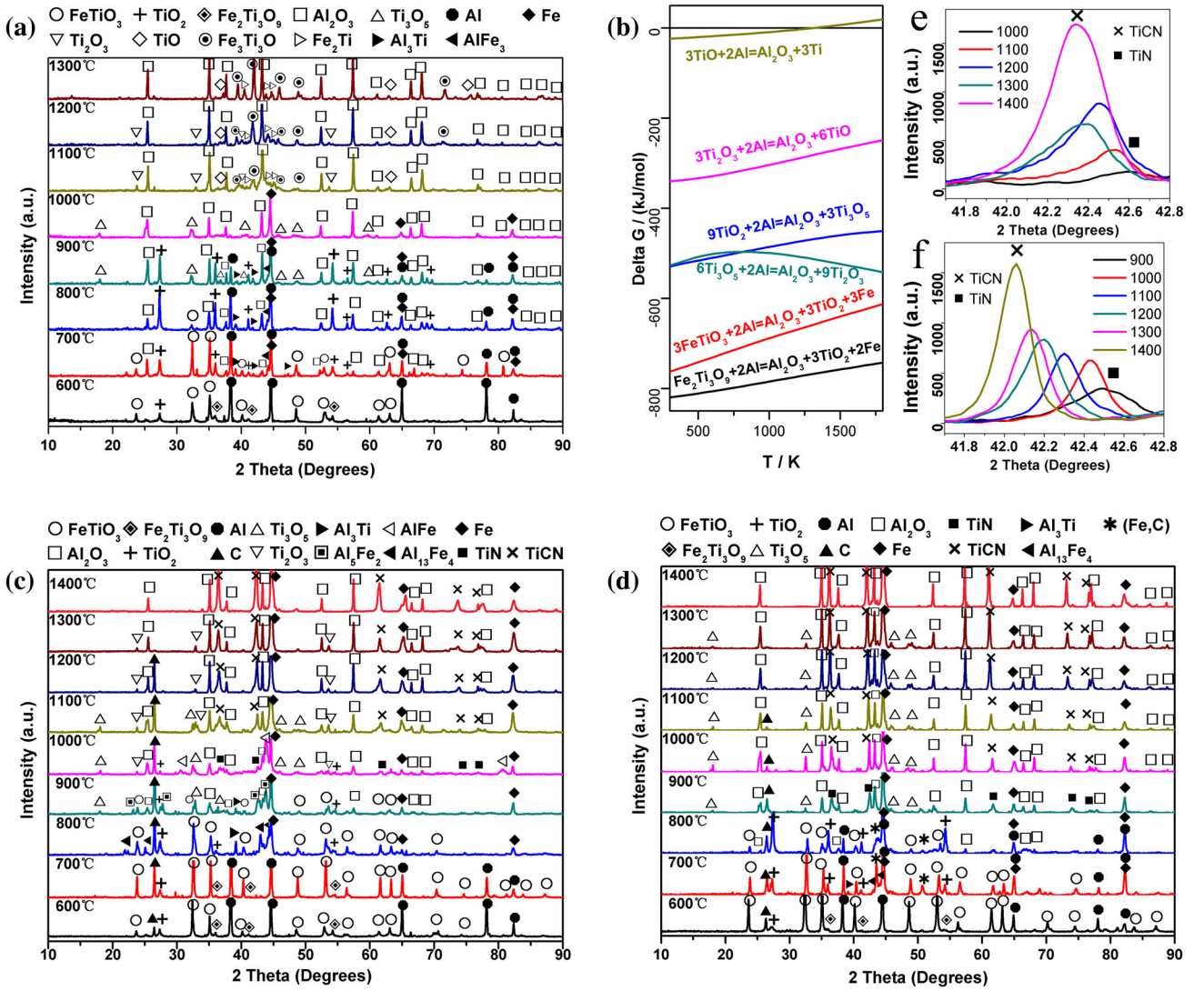

Fig. 2. XRD patterns of reaction process (a) $FeTiO_3$-2Al, (c) $FeTiO_3$-2Al-0.5C, and (d) $FeTiO_3$-2Al-0.75C; (b) ΔG-T curves of reactive process in the $FeTiO_3$-2Al system; enlarged XRD patterns showing the transition from TiN to TiCN with increasing temperature in the (e) $FeTiO_3$-2Al-0.5C and (f) $FeTiO_3$-2Al-0.75C system.

$$3Ti_3O_5 + 8Al + 9Fe = 3Fe_3Ti_3O + 4Al_2O_3 \quad (6)$$

$$3Ti_3O_5 + 10Al + 18Fe = 9Fe_2Ti + 5Al_2O_3 \quad \Delta G^\circ_{1000^\circ C} = -412\,kJ/Ti_3O_5 \quad (7)$$

$$6Ti_3O_5 + 2Al = 9Ti_2O_3 + Al_2O_3 \quad \Delta G^\circ_{1000^\circ C} = -65\,kJ/Ti_3O_5 \quad (8)$$

When the temperature was increased from 1100°C to 1300°C, no new phases appeared and the intensity of the TiO and Fe_3Ti_3O phases strengthened, accompanied by weakening of the Ti_2O_3 phase. Thus, Ti_2O_3 was further reduced to TiO and Fe_3Ti_3O by Al as the temperature was increased. In the $FeTiO_3$-2Al system, the Al content was theoretically sufficient to reduce all of the ilmenite to Ti. Al could not be found by XRD, probably due to its low content; however, Al was still present in the system. At the temperature of 1300°C, the final product was composed of Al_2O_3, Fe_3Ti_3O, Fe_2Ti, and TiO phases. The presence of Fe_3Ti_3O and TiO phases indicates that it was difficult for Al to reduce ilmenite to Ti completely. Figure 3 shows the thermodynamic process of ilmenite reduction by Al. As seen from Fig. 2b, in the process of aluminothermic reduction of ilmenite, the formation of TiO_2, Ti_3O_5, Ti_2O_3, and TiO can occur due to the negative ΔG°. However, the reaction by which TiO was reduced by Al, forming Ti, is difficult to carry out above 1000°C because of the positive ΔG°.

Figure 2c shows the XRD patterns of $FeTiO_3$-2Al-0.5C powder sintered at different temperatures for 0.5 h under pressure of 20 MPa and nitrogen atmosphere. Compared with the $FeTiO_3$-2Al system, there was not much change before the temperature was raised to 800°C. When the temperature was

Table II. Phases of $FeTiO_3$-2Al-xC powders sintered at different temperatures

Temperature (°C)	$FeTiO_3$-2Al	$FeTiO_3$-2Al-0.5C	$FeTiO_3$-2Al-0.75C
600	$FeTiO_3$, $Fe_2Ti_3O_9$, TiO_2, Al	$FeTiO_3$, $Fe_2Ti_3O_9$, TiO_2, Al, C	$FeTiO_3$, $Fe_2Ti_3O_9$, TiO_2, Al, C
700	$FeTiO_3$, TiO_2, Al, Al_2O_3, Al_3Ti, $AlFe_3$	$FeTiO_3$, $Fe_2Ti_3O_9$, TiO_2, Al, C	$FeTiO_3$, TiO_2, Al, Fe, Al_3Ti, $Al_{13}Fe_4$, (Fe, C), C
800	TiO_2, $FeTiO_3$, Al, Al_2O_3, Al_3Ti, $AlFe_3$, Fe	$FeTiO_3$, TiO_2, Al_3Ti, $Al_{13}Fe_4$, Fe, C	TiO_2, $FeTiO_3$, Al, Al_2O_3, Fe, (Fe, C), C
900	TiO_2, Ti_3O_5, Al, Al_2O_3, Al_3Ti, $AlFe_3$, Fe	TiO_2, Ti_3O_5, $FeTiO_3$, Al_3Ti, Al_5Fe_2, Al_2O_3, Fe, C	Ti_3O_5, TiN, Al_2O_3, Fe, C
1000	Ti_3O_5, Al_2O_3, Fe	Ti_3O_5, Ti_2O_3, TiO_2, TiN, AlFe, Al_2O_3, Fe, C	Ti_3O_5, TiCN, Al_2O_3, Fe, C
1100	Ti_2O_3, TiO, Fe_3Ti_3O, Fe_2Ti, Al_2O_3	Ti_3O_5, Ti_2O_3, TiCN, Al_2O_3, Fe, C	Ti_3O_5, TiCN, Al_2O_3, Fe, C
1200	TiO, Ti_2O_3, Fe_3Ti_3O, Fe_2Ti, Al_2O_3	Ti_2O_3, TiCN, Al_2O_3, Fe, C	Ti_3O_5, TiCN, Al_2O_3, Fe
1300	TiO, Fe_3Ti_3O, Fe_2Ti, Al_2O_3	Ti_2O_3, TiCN, Al_2O_3, Fe	Ti_3O_5, TiCN, Al_2O_3, Fe
1400		TiCN, Al_2O_3, Fe	TiCN, Al_2O_3, Fe

increased to 800°C, the Al peaks disappeared and two intermediate alloy phases appeared, i.e., Al_3Ti and $Al_{13}Fe_4$. The intermediate alloy $Al_{13}Fe_4$ phase was formed by the reaction of Al and the freshly formed Fe. When the temperature was increased to 900°C, the intensity of the TiO_2 phase became weaker, and Ti_3O_5 peaks appeared. In addition, the $Al_{13}Fe_4$ phase disappeared and another Al_5Fe_2 phase appeared. When the temperature was raised to 1000°C, the TiN and Ti_2O_3 phases and another AlFe phase appeared, and the peaks of the Al_5Fe_2 phase disappeared. At 1000°C, the AlFe phase disappeared completely. During this process, there were two notable changes. The first change was in the Al-Fe phase, such as $Al_{13}Fe_4$, Al_5Fe_2, and AlFe. Richards et al.[25] calculated that the intermediate alloy Al-Fe phase had negative Gibbs free energy at 700°C; therefore, thermodynamic formation of these Al-Fe phases is completely available. From the perspective of the reaction process, the Al-Fe phase would participate in the reaction to reduce TiO_2 when there was no Al in the system, as shown in Eqs. 9–15. The estimated data can be obtained according to the available thermodynamic data at 700°C. As seen from Eqs. 9–15, the Gibbs free energy of the reactions in which Al-Fe is involved is negative. Khoshhal et al.[3,5,26] also detected the Al_5Fe_2 phase in a study of the $FeTiO_3$-2Al and $FeTiO_3$-2Al-C systems and confirmed that the Al_5Fe_2 phase as a reducing agent would reduce TiO_2. However, the $Al_{13}Fe_4$ and AlFe phases were not detected in their research. The second change was the formation of TiN. The TiN phase was formed by the reaction between Ti_3O_5 and C under a nitrogen atmosphere. According to the reduction process of ilmenite by Al in the $FeTiO_3$-2Al system under nitrogen atmosphere, it is impossible to form TiN by aluminothermic reduction of the titanium oxides. In addition, many studies[27–29] have observed that Ti_3O_5 is easily converted to TiN in presence of C under nitrogen atmosphere.

$$15Al_{13}Fe_4 + 15FeTiO_3 = 15TiO_2 + 5Al_2O_3 + 37Al_5Fe_2 + Fe \quad (9)$$
$$\Delta G^\circ_{900^\circ C} = -273\,kJ/FeTiO_3$$

$$2Al_{13}Fe_4 + 27TiO_2 = 9Ti_3O_5 + 3Al_2O_3 + 4Al_5Fe_2 \quad (10)$$
$$\Delta G^\circ_{900^\circ C} = -58\,kJ/TiO_2$$

$$2Al_5Fe_2 + 9FeTiO_3 = 9TiO_2 + 3Al_2O_3 + 4AlFe + 9Fe \quad (11)$$
$$\Delta G^\circ_{1000^\circ C} = -223\,kJ/FeTiO_3$$

$$2Al_5Fe_2 + 27TiO_2 = 9Ti_3O_5 + 3Al_2O_3 + 4AlFe \quad (12)$$
$$\Delta G^\circ_{1000^\circ C} = -61\,kJ/TiO_2$$

$$2Al_5Fe_2 + 18Ti_3O_5 = 27Ti_2O_3 + 3Al_2O_3 + 4AlFe \quad (13)$$
$$\Delta G^\circ_{1000^\circ C} = -65\,kJ/Ti_3O_5$$

$$2AlFe + 9TiO_2 = 3Ti_3O_5 + Al_2O_3 + 2Fe \quad (14)$$
$$\Delta G^\circ_{1100^\circ C} = -58\,kJ/Ti_3O_5$$

$$2AlFe + 6Ti_3O_5 = 9Ti_2O_3 + Al_2O_3 + 2Fe \quad (15)$$
$$\Delta G^\circ_{1100^\circ C} = -59\,kJ/Ti_3O_5$$

When the temperature was increased from 1100°C to 1400°C, the intensity of Ti_2O_3 and C peaks weakened, and TiN was gradually transformed to the TiCN phase with increasing temperature. The titanium oxides completely disappeared at the temperature of 1400°C, and the final product was composed of Al_2O_3, TiCN, and Fe phases.

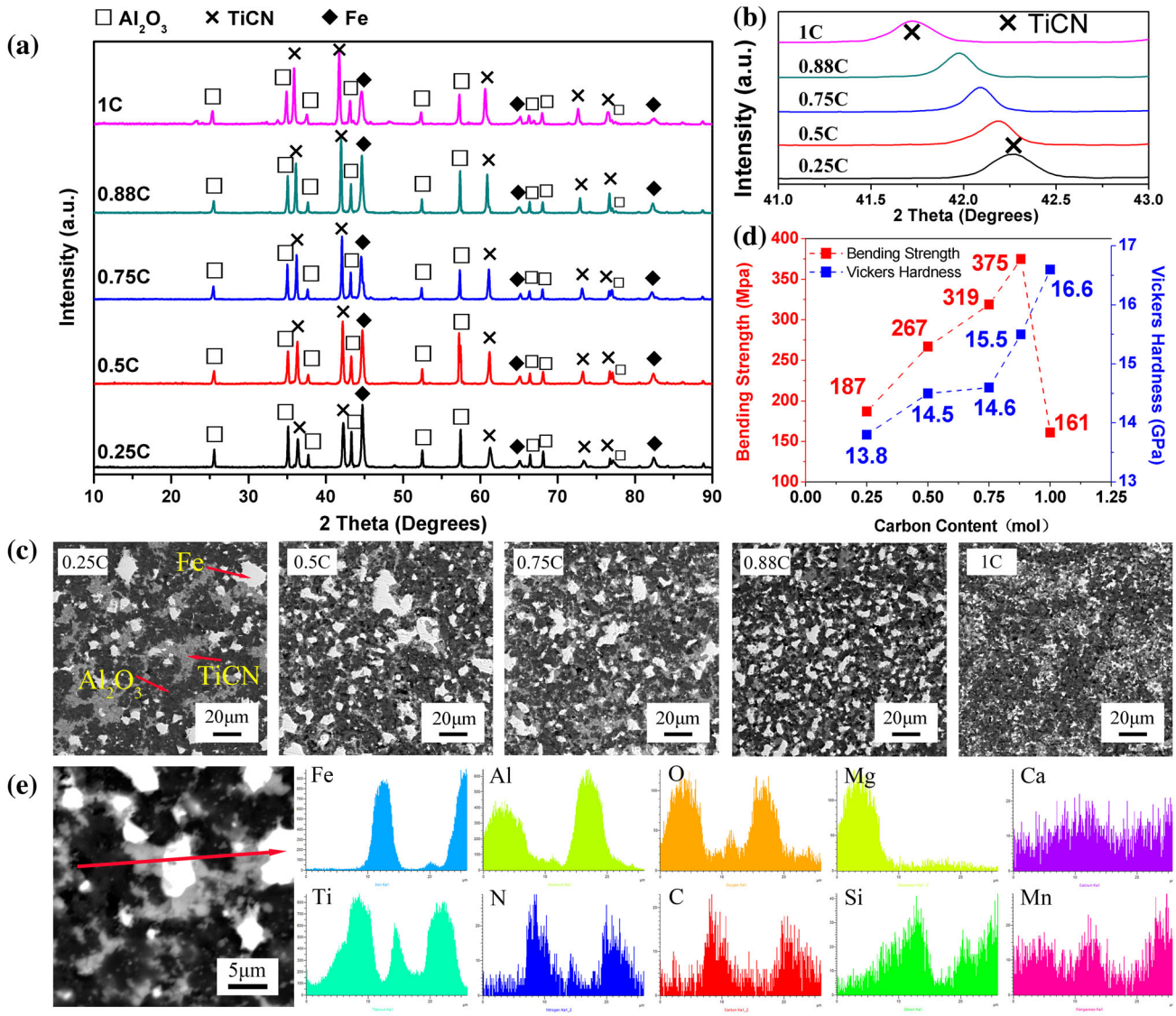

Fig. 3. (a) XRD patterns of $FeTiO_3$-2Al-*x*C powders sintered at 1400°C for 0.5 h; (b) Enlarged XRD patterns showing the effect of carbon content on the TiCN peak position; (c) Backscattered electron micrographs of sintered samples; (d) Bending strength and VH of sintered samples; (e) Elemental line scan spectra of the 0.5C sample.

Figure 2d shows the XRD patterns of $FeTiO_3$-2Al-0.75C powder sintered at different temperatures for 0.5 h under pressure of 20 MPa and nitrogen atmosphere. Compared with the $FeTiO_3$-2Al-0.5C system, the reaction process of the $FeTiO_3$-2Al-0.75C system was almost similar to that of the $FeTiO_3$-2Al-0.5C system. However, there were some major changes in the reduction process of the $FeTiO_3$-2Al-0.75C system. First, the formation temperature of TiN in the $FeTiO_3$-2Al-0.5C and $FeTiO_3$-2Al-0.75C systems was 1000°C and 900°C, respectively, indicating that enrichment of carbon tends to decrease the formation temperature of TiN during the sintering process. Second, the last intermediate titanium oxide that appeared in the $FeTiO_3$-2Al-0.5C and $FeTiO_3$-2Al-0.75C systems was Ti_2O_3 and Ti_3O_5, respectively, indicating that Ti_3O_5 was not further reduced to Ti_2O_3 but directly converted to TiN in the $FeTiO_3$-2Al-0.75C system. Many studies[29–31] have reported that Ti_2O_3 is very unstable in the carbothermal reduction process under nitrogen-containing atmosphere. However, it can be seen from study of the $FeTiO_3$-2Al-0.5C system that Ti_2O_3 could be stably present in the nitrogen atmosphere. Third, a new (Fe, C) phase appeared at 700°C in the $FeTiO_3$-2Al-0.75C system, due to the carbon solution in the iron. Carbon was dissolved in iron and diffused with iron as a transport medium, which favors the carbothermal reduction process. Once formation of TiC or TiN started, the fraction of (Fe, C) decreased as TiCN or TiN increased, which implies the onset of a reaction between (Fe, C) and reduced TiO_2.[32]

The study of the $FeTiO_3$-2Al-0.5C and $FeTiO_3$-2Al-0.75C systems showed that the reduction process of ilmenite was preceded by three main stages.

First, $FeTiO_3$ and $Fe_2Ti_3O_9$ were reduced by Al to form TiO_2 and Fe. TiO_2 was then reduced by Al to Ti_3O_5 or Ti_2O_3. Finally, Ti_3O_5 (or Ti_2O_3) was reduced by carbon to the cubic phase of TiN under nitrogen atmosphere, then the TiN phase gradually transformed to TiCN. This finding is in line with previous research[29,33,34] which identified that the reaction sequence of TiO_2 reduced by carbon was $TiO_2 \rightarrow Ti_nO_{2n-1} \rightarrow Ti_3O_5 \rightarrow TiC_xN_yO_{1-x-y}$ under nitrogen atmosphere.

Figure 2e and f show enlarged XRD patterns from Fig. 2c and d in the range of 41.7° to 42.8°, revealing the transition from TiN to TiCN with increasing temperature in the $FeTiO_3$-2Al-0.5C and $FeTiO_3$-2Al-0.75C system, respectively. As the temperature is increased, the TiN peaks shift to the left to smaller angle, indicating formation of TiCN. This peak shift corresponds to an increase in lattice parameter. The lattice parameters of the TiCN phase are presented in Table III.

Influence of Carbon Content on Phase, Microstructure, and Properties of Synthesis Products

Figure 3a shows the XRD patterns of the milled $FeTiO_3$-2Al-xC powders sintered at 1400°C for 0.5 h under pressure of 20 MPa and nitrogen atmosphere. After sintering at 1400°C, titanium oxide could not be detected by XRD, indicating that all of the titanium oxides were reduced to TiCN. The phases present in the final synthetic product were Al_2O_3, TiCN, and Fe.

Figure 3b shows the influence of the carbon content on the peak position of the TiCN phase, and Table IV presents the TiCN lattice parameter. As the carbon content was increased, the peak position of the TiCN phase shifted to the left and the lattice parameter of the TiCN phase also increased. On the one hand, in the process of carbon reduction of Ti_3O_5 (or Ti_2O_3) in nitrogen atmosphere, carbon and nitrogen atoms could gradually displace oxygen atoms of Ti_3O_5 (or Ti_2O_3) at high temperatures to form $TiC_xN_yO_{1-x-y}$, causing the peak position to shift further to the left.[35,36] On the other hand, at given reaction temperature, when the carbon content is increased, more carbon will participate in the reduction reaction and thus more oxygen atoms will be displaced by carbon and nitrogen atoms.[2,37] Consequently, the carbon and nitrogen content in the cubic phase increased, which is related to a significant increase in the lattice parameter because the TiC lattice parameter (0.4322 nm) is significantly higher than those of TiN (0.4242 nm) or TiO (0.4172 nm for $TiC_{0.006}O_{0.987}N_{0.007}$).[38] The results obtained in this work agree with this observation.

Backscattered electron images of sintered samples prepared from the $FeTiO_3$-2Al-xC systems are shown in Fig. 3c. The three different microstructure colors represent three different phases, i.e., Al_2O_3, TiCN, and Fe. These three phases were interlaced, and their distribution characteristics were not obvious. When the carbon content was low, the Al_2O_3, TiCN, and Fe phases clustered together and looked very coarse, especially the TiCN and Fe phases. With higher carbon content, the phases were observed to become smaller and the TiCN and Fe distribution was more uniform.

The bending strength and VH of samples sintered at 1400°C for 0.5 h under pressure of 20 MPa are shown in Fig. 3d. The VH value was observed to increase with increase in the carbon content. On the one hand, the grain size decreased as the carbon content was increased, resulting in an increase in hardness. On the other hand, according to the reduction process, the carbon was insufficient to completely reduce the oxygen in the TiCN when the carbon content was small, which resulted in TiCN's high oxygen content. The bending strength increased as the carbon content was increased, reaching a peak when the carbon content was 0.88 mol. When the carbon content was increased to 1 mol, the bending strength dropped sharply, due to residual carbon in the material. The ilmenite contained a little impurity which was difficult to be reduced by carbon; therefore, 1 mol of carbon was not completely consumed during the reaction. Under nitrogen atmosphere, the amount of carbon used in the synthesis of TiCN by carbothermal reduction was less than that of TiC, as shown in Eq. 1. This is confirmed by some studies[1,37] showing that high carbon content will lead to carbon residue in the material after synthesis of TiCN. When the carbon content was 0.88 mol, the synthetic products achieved comprehensive mechanical properties, i.e., bending strength and VH values of 375 MPa and 15.5 GPa, respectively.

Backscattered electron images and elemental line scan spectra of the 0.5C specimens are shown in Fig. 3e. The elemental line scan spectra confirm that the light-grayish particles are TiCN, because the distribution of the corresponding elements

Table III. Measured lattice parameters of TiCN at different temperatures in the $FeTiO_3$-2Al-0.5C and $FeTiO_3$-2Al-0.75C systems

Temperature (°C)	900	1000	1100	1200	1300	1400
Lattice parameter (Å) ($FeTiO_3$-2Al-0.5C)	–	–	4.2452	4.2474	4.2595	4.2613
Lattice parameter (Å) ($FeTiO_3$-2Al-0.75C)	4.2464	4.2547	4.2696	4.2780	4.2820	4.2886

Table IV. Lattice parameter of TiCN in $FeTiO_3$-2Al-xC system with different carbon contents

Carbon content	0.25	0.5	0.75	0.88	1
Lattice parameter (Å)	4.2507	4.2613	4.2886	4.3007	4.3140

overlapped (such as Ti, C, and N), while the dark-gray particles were Al_2O_3 and the white particles were Fe. In addition, the scanning results reveal the distribution of impurities, which were difficult to detect using XRD. The distribution curve of the Mg element can be seen to overlap with a part of the Al_2O_3 curve, suggesting that Mg impurity is generally distributed in Al_2O_3. Tang et al.[6] detected $MgAl_2O_4$ phase during the reduction process of the $FeTiO_3$-1Al-2.5C system because of the high content of Mg in ilmenite. In this work, the Mg and Al_2O_3 impurities were distributed together, but did not form a Mg-Al-O ternary phase because of low content of Mg impurities in ilmenite. The distribution characteristics of Si and Mn impurities were not obvious, according to their line scan curve distribution; most of them were dissolved in iron with a small part distributed on the phase boundary.

CONCLUSION

Al_2O_3-TiCN-Fe composites were synthesized by chemical reactions between natural ilmenite, aluminum, and carbon via a hot-pressing process. The aluminothermic reduction of ilmenite in the carbon-free $FeTiO_3$-2Al system was a gradual deoxygenation process. A series of intermediate titanium oxides were generated by the reduction of aluminum, i.e., TiO_2, Ti_3O_5, Ti_2O_3, TiO, Fe_3Ti_3O, and Fe_2Ti, according to the order of reduction. In the carbon-containing $FeTiO_3$-2Al-xC systems, TiN is generated with carbon involved in the reaction process, which will gradually transform to TiCN with increased temperature. The synthesis temperature of TiN decreased with increase of the carbon content in the system, being 1000°C and 900°C in the $FeTiO_3$-2Al-0.5C and $FeTiO_3$-2Al-0.75C system, respectively. Carbon could play an obvious role in grain refinement, and the grain size decreased and the distribution of TiCN and Fe became more uniform as the carbon content was increased. The system with 0.88 mol carbon resulted in comprehensive mechanical properties after sintering at 1400°C, i.e., bending strength and Vickers hardness of 375 MPa and 15.5 GPa, respectively.

ACKNOWLEDGEMENTS

The authors acknowledge financial support from The Ministry of Education "Chunhui Plan" Cooperative Research Project (16201417), the Key Research Project of Xihua University (Z1520102), Xihua University Key Laboratory Open Fund Project (SZJJ2014-061), and Scientific Research Project in Sichuan Province Department of Education (15201444).

REFERENCES

1. K.H. Wu, G.H. Zhang, and H.P. Gou, *Vacuum* 151, 51 (2018).
2. E. Ahmadi, A. Fauzi, H. Hussin, N. Baharun, K.S. Ariffin, and S.A. Rezan, *Int. J. Min. Met. Mater.* 24, 444 (2017).
3. R. Khoshhal, M. Soltanieh, and M.A. Boutorabi, *J. Alloys Compd.* 628, 113 (2015).
4. N.J. Welham, *J. Alloys Compd.* 274, 303 (1998).
5. R. Khoshhal, M. Soltanieh, and M.A. Boutorabi, *Int. J. Refract. Met. Hard Mater.* 45, 53 (2014).
6. A.T. Tang, S.M. Liu, and F.S. Pan, *Prog. Nat. Sci.* 23, 501 (2013).
7. N.J. Welham, T. Kerr, and P.E. Willis, *J. Am. Ceram. Soc.* 82, 2332 (1999).
8. Z. Yin, C. Huang, B. Zou, H. Liu, H. Zhu, and J. Wang, *Ceram. Int.* 39, 8877 (2013).
9. Z. Yin, C. Huang, B. Zou, H. Liu, H. Zhu, and J. Wang, *Mater. Sci. Eng. A* 577, 9 (2013).
10. M. Razavi, A.H. Rajabi-Zamani, M.R. Rahimipour, R. Kaboli, M.O. Shabani, and R. Yazdani-Rad, *Ceram. Int.* 37, 443–449 (2011).
11. J. Pourhosseini, M. Zakeri, M.R. Rahimipour, E. Salahi, and GhR Pourhosseini, *Mater. Sci. Technol. Lond.* 26, 1132 (2010).
12. M. Kholghy, S. Kharatyan, and H. Edris, *J. Alloys Compd.* 502, 491 (2010).
13. T. Nukami and M.C. Flemings, *Metall. Mater. Trans. A* 26, 1877 (1995).
14. H. Soda, Q. Xia, A. McLean, A.K. Pramanick, and G. Motoyasu, *Mater. Sci. Eng. A* 216, 61 (1996).
15. B.S.S. Daniel, V.S.R. Murthy, and G.S. Murty, *J. Mater. Sci. Technol.* 68, 132 (1997).
16. P.E. Willis, N.J. Welham, and A. Kerr, *J. Eur. Ceram. Soc.* 18, 701 (1998).
17. M. Razavi, M.R. Rahimipour, T. Ebadzadeh, and S.S.R. Tousi, *Bull. Mater. Sci.* 32, 155 (2009).
18. Z.G. Zou, C.Q. Yin, Y. Wu, and X.M. Li, *Key Eng. Mater.* 280–283, 1501 (2007).
19. Z.G. Zou, Y. Wu, C.Q. Yin, and X.M. Li, *J. Wuhan Univ. Technol. Mater. Sci. Ed.* 22, 706 (2007).
20. Z.G. Zou, J.L. Li, and Y. Wu, *Key Eng. Mater.* 280–283, 1103 (2005).
21. S. Alamolhoda, S. Heshmati-Manesh, and A. Ataie, *Adv. Powder Technol.* 23, 343 (2012).
22. Y.F. Shen, Z.G. Zou, Z.G. Xiao, K. Liu, F. Long, and Y. Wu, *Mater. Sci. Eng. A* 528, 2100 (2011).
23. V.P. Kobyakov, N.V. Sachkova, and M.A. Sichinava, *Inorg. Mater.* 46, 1396 (2010).
24. J.J.S. Dilip, B.S.B. Reddy, S. Das, and K. Das, *J. Alloys Compd.* 475, 178 (2009).
25. R.W. Richards, R.D. Jones, P.D. Clements, and H. Clarke, *Int. Mater. Rev.* 39, 191 (1994).
26. R. Khoshhal, M. Soltanieh, and M.A. Boutorabi, *Int. J. Refract. Met. Hard Mater.* 52, 17 (2015).
27. D.P. Xiang, Y. Liu, M.J. Tu, Y.Y. Li, and W.P. Chen, *Int. J. Refract. Met. Hard Mater.* 27, 111 (2009).
28. H. Kwon and S. Kang, *J. Am. Ceram. Soc.* 92, 272 (2009).
29. A. Jha and S.J. Yoon, *J. Mater. Sci.* 34, 307 (1999).
30. L.M. Berger, *J. Hard Mater.* 3, 3 (1992).

31. L.M. Berger, *J. Mater. Sci. Lett.* 20, 1845 (2001).
32. N.J. Welham and J.S. Williams, *Metall. Mater. Trans. B* 30, 1075 (1999).
33. W.Y. Li and F.L. Riley, *J. Eur. Ceram. Soc.* 8, 345 (1991).
34. R.M. Ren, Z.G. Yang, and L.L. Shaw, *Mater. Sci. Eng. A* 286, 65 (2000).
35. H.P. Gou, G.H. Zhang, and K.C. Chou, *Metall. Mater. Trans. B* 46B, 48 (2015).
36. S.A. Rezan, G. Zhang, and O. Ostrovski, *ISIJ Int.* 52, 363 (2012).
37. H.P. Gou, G.H. Zhang, X. Yuan, and K.C. Chou, *ISIJ Int.* 56, 744 (2016).
38. G. Neumann, R. Kieffer, and P. Ettmayer, *Monatsh. Chem.* 103, 1130 (1972).